Effect of Concentration of Nd3+ on the Photoluminescence and Ferroelectric Properties of Bi4-xNdxTi3O12 Films

Yudong Xu
Hefei University of Technology
Kunzhuang Hu
Hefei University of Technology
Min Shi (hfutdou@hotmail.com)
Hefei University of Technology https://orcid.org/0000-0002-2870-5016
Ruzhong Zuo
Hefei University of Technology
Guannan Qiu
Hefei University of Technology
Zhuolin Si
Hefei University of Technology
Enyang Men
Hefei University of Technology

Research Article

Keywords: spin-coating methods, maximal remanent polarization, blue light emission peak

Posted Date: February 22nd, 2021

DOI: https://doi.org/10.21203/rs.3.rs-214347/v1

Effect of concentration of Nd^{3+} on the photoluminescence and ferroelectric properties of $Bi_{4-x}Nd_xTi_3O_{12}$ films

Yudong Xu[1], Kunzhuang Hu[1], Min Shi[1,*], Ruzhong Zuo[1], Guannan Qiu[1], Zhuolin Si[1] and Enyang Men[1]

[1] School of Materials Science and Engineering, Hefei University of Technology, Hefei 230069, China

ABSTRACT: Lead-free films of $Bi_{4-x}Nd_xTi_3O_{12}$ were deposited on Pt(111)/Ti/SiO_2/Si(100) substrate via spin-coating methods. It is shown that there are no secondary phases in $Bi_{4-x}Nd_xTi_3O_{12}$ films and clear interfaces between the $Bi_{4-x}Nd_xTi_3O_{12}$ films and substrates when the films are annealed at 700 ℃. And the $Bi_{4-x}Nd_xTi_3O_{12}$ films also exhibit a blue light emission peak at 437 nm and a yellow light emission peak at 580 nm. There are narrower band gaps, higher dielectric constant and lower dielectric loss when Nd^{3+} concentration varies from 0 to 0.85. And the $Bi_{3.15}Nd_{0.85}Ti_3O_{12}$ film possesses the minimum of band gap energy (2.67 eV). Moreover, $Bi_{3.55}Nd_{0.45}Ti_3O_{12}$ film exhibits a minimal leakage current density and a maximal remanent polarization, which is highly beneficial for the potential applications in multi-functional devices.

1 Introduction

Since the ferroelectricity in Rochelle salt crystals was discovered by French Valasek in 1920, ferroelectric materials have become a research hotspot [1] and been widely used in transducers, filters, resonators, ferroelectric memories and other fields [2-6]. Up to date, the widely used ferroelectric materials are lead-based because of their stable and excellent ferroelectric properties [7-10]. However, lead-based ferroelectric materials undesirably bring about harm to human beings and pollution to environment during the preparation and application processes. As a result, researchers have been looking for alternative lead-free high performance ferroelectric materials to rival the lead-based ferroelectrics such as $PbZr_xTi_{1-X}O_3$ [11].

Bismuth titanate ($Bi_4Ti_3O_{12}$), a typical lead-free multiferroics, has drawn widespread attention owing to its high Curie temperature and excellent fatigue

Address correspondence to E-mail: hfutdou@hotmail.com

resistance [12-14]. Unfortunately, its remnant polarization is rather low because of the evaporation of Bi^{3+} in the system, which gives rise to the increase of concentration of oxygen vacancies and the deterioration of ferroelectricity [15]. Thus, more and more researchers have been trying to inhibit the evaporation of Bi^{3+} through doping of rare elements in $Bi_4Ti_3O_{12}$ [16-18]. M. Chen [19] reported that the substitution of Pr^{3+} for Bi^{3+} will decrease the space charge density which improves ferroelectric properties of $Bi_4Ti_3O_{12}$ materials. And C. P. Cheng [20] reported that the doping of Dy^{3+} will enhance the ferroelectric properties of $Bi_4Ti_3O_{12}$. U. Chon [21] and X. Y. Mao [22] pointed that the doping of Nd^{3+} in $Bi_4Ti_3O_{12}$ can also enhance the ferroelectric properties. The reason is that the substitution of Nd^{3+} for Bi^{3+} causes obvious structural distortion along the C axis, thus resulting in a large polarization along the C axis [21, 23] besides inhibiting the evaporation of Bi^{3+}. Surprisingly, $Bi_4Ti_3O_{12}$ materials doped with rare earth elements possess obvious photoluminescence [24, 25]. R. Bokolia [26] reported that Er^{3+}-doped $Bi_4Ti_3O_{12}$ materials possess photoluminescence besides ferroelectric properties. And K. Ruan [27] pointed that Eu^{3+}-doped $Bi_4Ti_3O_{12}$ films possess good photoluminescent properties. Although, up to date, ferroelectric properties of Nd^{3+}-doped $Bi_4Ti_3O_{12}$ films have been investigated, there are few reports on investigating photoluminescence of Nd^{3+}-doped $Bi_4Ti_3O_{12}$ films. Therefore, it is necessary to study not only ferroelectric properties but also photoluminescence of Nd^{3+}-doped $Bi_4Ti_3O_{12}$ films systematically.

In this work, $Bi_{4-x}Nd_xTi_3O_{12}$ films were prepared on the substrates ($Pt(111)/Ti/SiO_2/Si(100)$) via the sol-gel and spin-coating method. And impact of the concentration of Nd^{3+} in $Bi_{4-x}Nd_xTi_3O_{12}$ films on the ferroelectric properties, dielectric properties, leakage current densities and photoluminescence were investigated. Photoluminescence and ferroelectric properties were studied in detail.

2 Experimental

The $Bi_{4-x}Nd_xTi_3O_{12}$ (when x=0, 0.25, 0.45, 0.65, 0.85) films were deposited on the $Pt(111)/Ti/SiO_2/Si(100)$ substrate, and precursors were fabricated by sol-gel method. Neodymium oxide (Nd_2O_3), bismuth nitrate pentahydrate ($Bi(NO_3)_3{\cdot}5H_2O$) and tetrabutyl titanate ($Ti(OC_4H_9)_4$) were selected as starting materials. 2-methoxyethanol

($C_3H_8O_2$) and acetic acid ($C_2H_4O_2$) were used as the solvents. Acetylacetone ($C_5H_8O_2$) was used to stabilize the solution. Firstly, certain proportion of Nd_2O_3 and $Bi(NO_3)_3{\cdot}5H_2O$ were dissolved in $C_2H_4O_2$ according to the stoichiometry of $Bi_{4-x}Nd_xTi_3O_{12}$. Thus, solution A was obtained. And excessive $Bi(NO_3)_3{\cdot}5H_2O$ (8 wt%) was used to compensate the loss of Bi^{3+} volatilization during annealing process. Then, $Ti(OC_4H_9)_4$ was dissolved in $C_3H_8O_2$, and a small quantity of stabilizer ($C_5H_8O_2$) was dripped into $C_3H_8O_2$. Then solution B was obtained. Then, the above two solutions (A and B) were mixed to get sol. And the sol was deposited on the substrates to get monolayered $Bi_{4-x}Nd_xTi_3O_{12}$ films via spin-coating technology. Subsequently, $Bi_{4-x}Nd_xTi_3O_{12}$ films were pre-annealed and annealed in tube furnace. At last, the above-mentioned process needs to be repeated three times to acquire four-layered $Bi_{4-x}Nd_xTi_3O_{12}$ films. The specific process was displayed in Fig. 1.

The phase constitutions of $Bi_{4-x}Nd_xTi_3O_{12}$ films were carried out by X-ray diffraction (X 'Pert Pro MPD, PANalytical, Holland). The morphologies of the surface and cross-section were investigated though FESEM (SU8020, Hitachi, Japan). P-E hysteresis loops of the films were determined by Precision LC Unit (Radiant Precision LC, Radiant Technologies, USA). The leakage current densities were determined by semiconductor tester (Keithley, 4200-SCS, USA). Absorption spectrum of films were obtained by the UV spectrophotometer (Cary-5000, Agilent, USA). Photoluminescent spectrum of the films were measured via fluorescence spectrophotometer (F4500, Hitachi, Japan).

3 Results and discussion

3.1 Phase constitution

The XRD patterns of five films of $Bi_{4-x}Nd_xTi_3O_{12}$ were displayed in Fig. 2. As shown in Fig. 2. (a), it is obvious that the diffraction peaks of the $Bi_{4-x}Nd_xTi_3O_{12}$ films are composed of those from $Bi_4Ti_3O_{12}$ (JCPDS No.72-1019) and from Pt on the top layer of the substrates without any from impurity phases [28, 29]. It indicates that Nd^{3+} has dissolved into the crystal lattice of $Bi_4Ti_3O_{12}$ and pure $Bi_{4-x}Nd_xTi_3O_{12}$ films have been prepared [30, 31]. And the sharp peaks imply good crystallinity [26]. As

shown in Fig. 2(b), for all the five films, the diffraction peaks at about 30.0° shift slightly to a greater angle. This is mainly due to the fact that the radius of Nb^{3+} (1.11 Å) is less than that of Bi^{3+} (1.17 Å) [22, 32]. The replacement of Bi^{3+} with Nd^{3+} will lead to reduction of lattice parameters and crystal plane spacing, and thus the diffraction peaks shift to a greater angle according to Bragg equation.

3.2 Microstructure

The surface graphs of the films were illustrated in the Fig. 3. It is seen that, for the $Bi_{4-x}Nd_xTi_3O_{12}$ films (x being 0 and 0.25, respectively), there are obvious cracks and pores on the surfaces of these samples. However, for the other films, cracks and pores are not found. With the increase of Nd^{3+} concentration, the particle sizes decrease and the relative density of $Bi_{4-x}Nd_xTi_3O_{12}$ films increases.

The cross-section images of $Bi_{4-x}Nd_xTi_3O_{12}$ films were shown in Fig. 4. All of the five films exhibit layered structure. The interfaces between $Bi_{4-x}Nd_xTi_3O_{12}$ films and substrates are flat. And there are no inter-layers between the films and substrates, implying that no diffusion exists between the $Bi_{4-x}Nd_xTi_3O_{12}$ films and substrates. It can be observed that the thicknesses of $Bi_{4-x}Nd_xTi_3O_{12}$ films are all around 200 nm, which is higher than that of pure $Bi_4Ti_3O_{12}$ film. The difference in thicknesses for $Bi_{4-x}Nd_xTi_3O_{12}$ films with different Nd^{3+} concentration is mainly due to the preparation of films by spin-coating technology.

3.3 Ferroelectric properties

The hysteresis loops of $Bi_{4-x}Nd_xTi_3O_{12}$ films were displayed in Fig. 5. The results obtained from Fig. 5 were listed in Tab. 1. $Bi_{4-x}Nd_xTi_3O_{12}$ films seem to exhibit good ferroelectric properties. The values of remnant polarization (*Pr*) and saturated polarization (*Ps*) of $Bi_{4-x}Nd_xTi_3O_{12}$ films are great than those of un-doped $Bi_4Ti_3O_{12}$ film, which indicates that doping of Nd^{3+} is beneficial for the improvement of the ferroelectric properties. It is seen that, firstly, the values of *Pr* increase to 16.86 $\mu c \cdot cm^{-2}$ and then decrease gradually with increasing Nd^{3+} concentration. The $Bi_{3.55}Nd_{0.45}Ti_3O_{12}$ film possesses the maximal value of *Pr* (16.86 $\mu c \cdot cm^{-2}$) which is greater than those of $Bi_4Ti_3O_{12}$ films in Ref. [33] (10.5$\mu c \cdot cm^{-2}$) and Ref. [34] (10

μc·cm^{-2}). And it is also significantly greater than un-doped $Bi_4Ti_3O_{12}$ films in Ref. [35] (4.8 μc·cm^{-2}).

In addition, it is worth noting that volatilization of Bi^{3+} during annealing process inevitably brings about increased oxygen vacancies and degraded ferroelectric properties of the films [28, 30]. The doping of a small amount of Nd^{3+} will inhibit the volatilization of Bi^{3+} and reduce the concentration of oxygen vacancies, and thus increase the values of *Pr*, as shown in Fig. 5. However, with the further increase of Nd^{3+} concentration, particle size will decrease and the values of *Pr* reduce correspondingly owing to the pinning effect [29, 34]. Therefore, The $Bi_{3.55}Nd_{0.45}Ti_3O_{12}$ film possesses the maximal value of *Pr*.

3.4 Leakage current densities

The leakage current densities of $Bi_{4-x}Nd_xTi_3O_{12}$ films were displayed in Fig. 6. Obviously, when the values of applied electric field (*E*) are below 100 KV·cm^{-1}, the leakage current densities increase rapidly with increasing *E*. However, when the values of *E* are greater than 100 KV·cm^{-1}, the leakage current densities increase slowly and remain constant finally. Compared with the $Bi_4Ti_3O_{12}$ film, Nd^{3+}-doped films possess lower leakage current densities, indicating that doping of Nd^{3+} is beneficial for the reduction of leakage current densities. The reason is that volatilization of Bi^{3+} during the annealing process induces higher concentration oxygen vacancies [36]. And the substitution of Nd^{3+} for Bi^{3+} inhibits the volatilization of Bi^{3+} effectively, thus reducing oxygen vacancies and leakage current densities. The data summarized from Fig. 6 were shown in Tab. 2. Among the five films, $Bi_{3.55}Nd_{0.45}Ti_3O_{12}$ film possesses the minimum of leakage current density (1.02×10^{-6} A·cm^{-2}), which is close to the data from Ref. [32] (2×10^{-6} A·cm^{-2}) and lower than those from Ref. [37] (1.15×10^{-5} A·cm^{-2}). It should be noted that leakage current density of $Bi_{3.55}Nd_{0.45}Ti_3O_{12}$ films is about one order lower than that of $Bi_4Ti_3O_{12}$ film (1.85×10^{-5} A·cm^{-2}).

3.5 Dielectric properties

Variation of dielectric constant (ε) and dielectric loss ($tan\delta$) with frequency was

shown in Fig. 7. As shown in Fig. 7(a), at lower frequency (<10000 Hz), the values of ε decrease rapidly with increasing frequency. Nevertheless, at higher frequency (>10000 Hz), the values of ε decrease slowly and remain nearly constant. It is clearly seen from Fig. 7(b) that, with increasing frequency, the values of *tanδ* remain nearly unchanged when frequency is smaller than 10000 Hz and increase rapidly when frequency is above 10000 Hz. At the same frequency, the values of ε increase and the values of *tanδ* decrease with the increase of Nd^{3+} concentration. This indicates that doping of Nd^{3+} can effectively enhance the dielectric properties of the films.

3.6 Photoluminescence

Excitation spectra of $Bi_{4-x}Nd_xTi_3O_{12}$ films were shown in Fig. 8(a). Obviously, there is a distinct excitation peak at about 294 nm, which corresponds to the energy level transition of $^4I_{9/2} \rightarrow {}^2H_{11/2}$ [38, 39]. The emission spectra of $Bi_{4-x}Nd_xTi_3O_{12}$ films were illustrated in Fig. 8(b), showing that there is one blue light emission peak at 437 nm and one yellow light emission peak at 580 nm. These are attributed to the energy level transitions of $^4G_{9/2} \rightarrow {}^4F_{9/2}$ and $^4G_{7/2} \rightarrow {}^4F_{9/2}$, respectively [38, 39]. The wavelength of the emission peaks almost doesn't change under different doping concentration of Nd^{3+}. With increasing concentration of Nd^{3+}, the emission intensities increase firstly and then decrease. The emission intensity reaches the maximum when the concentration of Nd^{3+} is equal to 0.45, which indicates quenching concentration is about 0.45. Concentration quenching mechanism is highly relevant to the critical interaction distance between neighboring activators in the host lattice [40, 41].

Next, we give an intuitive description on the luminescence mechanism of the $Bi_{4-x}Nd_xTi_3O_{12}$ films based on the possible partial energy level diagram of Nd^{3+}, as shown in Fig. 8(c). It can be clearly seen that Nd^{3+} was excited from ground state ($^4I_{9/2}$) to excited state ($^2H_{11/2}$) when excited at a deep ultraviolet light (DUV, 294nm). Then, Nd^{3+} was relaxed from excited state of $^2H_{11/2}$ to the energy level of $^4G_{9/2}$ and $^4G_{7/2}$ via non-radiative-relaxation [39, 41]. Finally, the electronic transitions from energy level of $^4G_{9/2}$ and $^4G_{7/2}$ to the energy level of $^4F_{9/2}$ give rise to a blue light emission peak at 437 nm and a yellow light emission peak at 580 nm, respectively.

The diagrams of Commission Internationale de L'Eclairage (CIE) chromaticity

coordinate of $Bi_{4-x}Nd_xTi_3O_{12}$ films were shown in Fig 9. It can be found that CIE chromaticity coordinates of $Bi_{3.75}Nd_{0.25}Ti_3O_{12}$, $Bi_{3.55}Nd_{0.45}Ti_3O_{12}$, $Bi_{3.35}Nd_{0.65}Ti_3O_{12}$ and $Bi_{3.15}Nd_{0.85}Ti_3O_{12}$ are (0.2568, 0.2545), (0.2402, 0.2552), (0.2509, 0.2610), (0.2499, 0.2688), respectively, which are all in the blue region of the CIE diagram.

The ultraviolet (UV) -visible (Vis) -near infrared (NIR) absorption spectra of $Bi_{4-x}Nd_xTi_3O_{12}$ films were shown in Fig. 10(a). It can be seen that the films exhibit obvious absorptions from 350 nm to 500 nm. In general, for the indirect transitions, the band gap energy (*Eg*) can be obtained via following formula [42, 43]:

$$\alpha h\nu^{1/2} = A(h\nu - Eg) \quad (1)$$

Where α is the absorption coefficient from the absorption spectrum, *A* is constant and *hv* is energy of a photon, respectively. Variations of $(\alpha hv)^{1/2}$ with *hv* of the films were shown in Fig. 10(b). The values of *Eg* will be determined from the intersections of the curve tangent and the abscissa [44, 45], as shown in Tab.3. Apparently, the values of *Eg* decrease gradually with the increase of Nd^{3+} concentration, which is beneficial for enhancing visible light catalytic activity [42, 44]. The value of *Eg* of $Bi_{3.15}Nd_{0.85}Ti_3O_{12}$ film is 2.67 eV, which is smaller than that reported in Ref. [42] (2.82 eV), which implies the potential application in light catalytic fields as smaller *Eg* is beneficial for enhancing visible light catalytic activity [42, 44].

4 Conclusions

$Bi_{4-x}Nd_xTi_3O_{12}$ films doped with different concentrations of Nd^{3+} were deposited on the substrate via spin-coating technology. The as-prepared $Bi_{4-x}Nd_xTi_3O_{12}$ films are pure and have very few pores and cracks on the surfaces of the films. The interfaces between $Bi_{4-x}Nd_xTi_3O_{12}$ films and the substrates are clear and flat. $Bi_{3.55}Nd_{0.45}Ti_3O_{12}$ film possess the maximum of *Pr* (16.86 $\mu c \cdot cm^{-2}$) and the minimum of leakage current density (1.02×10^{-6} $A \cdot cm^{-2}$). With the increase of Nd^{3+} concentration, the values of ε of the films increase and the values of $tan\delta$ decrease. The films of $Bi_{4-x}Nd_xTi_3O_{12}$ exhibit a blue light emission peak at 437 nm and a yellow light emission peak at 580 nm. With increasing concentration of Nd^{3+}, the values of *Eg* decrease gradually. For the film of $Bi_{3.15}Nd_{0.85}Ti_3O_{12}$, the value of band gap energy is 2.67 eV. The

photoluminescence and ferroelectric properties of $Bi_{3.55}Nd_{0.45}Ti_3O_{12}$ film are, on the whole, good and helpful for the applications in multi-functional devices.

Acknowledgments

The authors acknowledge the financial support from The National Natural Science Foundation of China (52072103).

Compliance with ethical standards

Conflict of interest The authors declare no conflict of interest.

References

[1] B. Fugiel, S. Komraus, T. Kikuta, Influence of side electric potential on hysteresis loop parameters and electric permittivity in the rochelle salt. Physica. B. **407**, 3956-3959 (2012).

[2] W. T. Chen, A. E. Gurdal, S. Tuncdemir, J. Gambal, C. A. Randall, Introducing an extremely high output power and high temperature piezoelectric bimorph energy harvester technology based on the ferroelectric system $Bi(Me)O_3$-$PbTiO_3$. J. Appl. Phys. **128**, 144102 (2020).

[3] M. Z. Koohi, A. Mortazawi, Negative piezoelectric based electric-field-actuated mode-switchable multilayer ferroelectric FBARs for Selective control of harmonic resonances without degrading keff. IEEE. T. Ultrason. Ferr. **67**, 1922-1930 (2020).

[4] J. Wang, M. Park, S. Mertin, T. Pensala, F. Ayazi, A. Ansari, A film bulk acoustic resonator based on ferroelectric aluminum scandium nitride films. J. Microelectromech. S. **29**, 741-747(2020).

[5] X. Qiao, W. Geng, D. Zheng, X. Chou, Robust in-plane polarization switching in epitaxial $BiFeO_3$ films. J. Alloy. Compd. **852**, 156988(2020).

[6] P. Pandey, S. H. Wan, K. R. Udayakumar, T. S. Moise, A. C. Seabaugh, Programming-pulse dependence of ferroelectric partial polarization: insights from a comparative study of PZT and HZO capacitors. IEEE. T. Electron. Dev. **67**, 4482-4487 (2020).

[7] R. Indergand, A. Vidyasagar, N. Nadkarni, D. M. Kochmann, A phase-field approach to studying the temperature-dependent ferroelectric response of bulk polycrystalline PZT. J. Mech. Phys. Solids. **144**, 104098 (2020).

[8] S. A. Sharko, A. I. Serokurova, N. N. Novitskii, V. A. Ketsko, A. I. Stognij, Continuous ferrimagnetic $Y_3Fe_5O_{12}$ layers on the ceramic $PbZr_{0.45}Ti_{0.55}O_3$ substrates. Ceram. Int. **46**, 22049-22056 (2020).

[9] B. Gao, Z. H. Yao, D. Y. Lai, Q. H. Guo, W. G. Pan, H. Hao, M. H. Cao, H. X. Liu, Unexpectedly high piezoelectric response in Sm-doped PZT ceramics beyond the morphotropic phase boundary region. J. Alloy. Compd. **836**, 155474 (2020).

[10] P. Kumar, C. Prakash, Synthesis, dielectric and ferroelectric properties of Sm^{3+} modified PZTFN ceramics. Mater. Chem. Phys. **251**, 123061 (2020).

[11] H. Wang, H. Yuan, X. Liu, K. Wu, D. Lin, Achieving high energy-storage properties in $Bi_{0.5}Na_{0.5}TiO_3$-based lead-free ceramics under low electric fields. Ceram. Int. **47**, 1344-1352 (2020).

[12] M. A. Wederni, D. B. Jemia, H. Rahmouni, R. J. Martin-Palma, R. Chtourou, Structural, morphological, vibrational, and impedance properties of ytterbium modified bismuth titanate. Chem. Phys. Lett. **755**, 137787 (2020).

[13] M. Alguero, M. Perez-Cerdan, P. R. D. Real, J. Ricote, A. Castro, Novel aurivillius $Bi_4Ti_{3-2x}Nb_xFe_xO_{12}$ phases with increasing magnetic-cation fraction until percolation: a novel approach for room temperature multiferroism. J. Mater. Chem. C. **836**, 12457-12469 (2020).

[14] C. B. Long, H. Q. Fan, W. Ren, J. Y. Zhao, Double polarization hysteresis and dramatic influence of small compositional variations on the electrical properties in $Bi_4Ti_3O_{12}$ ceramics. J. Eur. Ceram. Soc. **39**, 4103-4112 (2019).

[15] R. Nie, J. Yuan, Q. Chen, J. Xing, J. Zhu, W. Zhang, Crystal distortion and electrical properties of Ce-doped BIT-based piezoelectric ceramics. J. Am. Ceram. Soc. **102**, 5432-5442 (2019).

[16] S. Ma, X. W. Cheng, T. Ali, Tayyeb, Influence of tantalum on mechanical, ferroelectric and dielectric properties of Bi-excess $Bi_{3.25}La_{0.75}Ti_3O_{12}$ thin film. Appl. Surf. Sci. **463**, 1141-1147 (2019).

[17] C. Y. Yau, R. Palan, K. Tran, R. C. Buchanan, Mechanism of polarization enhancement in La-doped $Bi_4Ti_3O_{12}$ films. Appl. Phys. Lett. **86**, 032907 (2005).

[18] Y. Y. Wu, X. H. Wang, L. T. Li, Ferroelectric and dielectric properties of La/Mn co-doped $Bi_4Ti_3O_{12}$ ceramics. Chinese. Phys. B. **19**, 037701 (2010).

[19] M. Chen, Z. L. Liu, Y. Wang, C. C. Wang, X. S. Yang, K. L. Yao, Ferroelectric properties of Pr_6O_{11}-doped $Bi_4Ti_3O_{12}$. Solid. State. Commun. **130**, 735–739 (2004).

[20] C. P. Cheng, M. H. Tang, Z. Ye, Y. C. Zhou, Ferroelectric properties of dysprosium-doped $Bi_4Ti_3O_{12}$ thin films crystallized in various atmospheres. T. Nonferr. Metal. Soc. **16**, S33-S36 (2006).

[21] U. Chon, J. S. Shim, H. M. Jang, Compositional dependence of ferroelectric properties of highly c-axis oriented $Bi_{4-x}Nd_xTi_3O_{12}$ film capacitors. Solid. State. Commun. **129**, 465–468 (2004).

[22] X. Y. Mao, F. W. Mao, X. B. Chen, Ferroelectric and dielectric properties of $Bi_{4-x}Nd_xTi_3O_{12}$ ceramics. Integr. Ferroelectr. **79**, 155-161 (2006).

[23] Y. Ahn, J. Y. Son, Mixed grains and orientation-dependent piezoelectricity of polycrystalline Nd-substituted $Bi_4Ti_3O_{12}$ thin films. Ceram. Int. 42, 13061-13064 (2016)

[24] F. Gao, H. F. Liu, F. Ren, K. T. Wang, X. S. Li, Y. B. Wang, C. L. He, Y. Z. Wei, Tunable structure and intensive upconversion photoluminescence for Ho^{3+}-Yb^{3+} codoped bismuth titanate composite synthesized by sol-gel-combustion (SGC) method. Cream. Int. **46**, 3015-3022 (2020).

[25] F. M. Yang, B. Jia, T. Wei, C. Z. Zhao, Q. J. Zhou, Z. P. Li, M. R. Du, M. C. Wang, Y. Y. Liu, C. Y. Xie, Reversible regulation of upconversion luminescence in new photochromic ferroelectric materials: $Bi_{4-x}Er_xTi_3O_{12}$ ceramics. Inorg. Chem. Front. **6**, 2756-2766 (2019).

[26] R. Bokolia, O. P. Thakur, V. K. Rai, S. K. Sharma, k. Sreenivas, Dielectric, ferroelectric and photoluminescence properties of Er^{3+} doped $Bi_4Ti_3O_{12}$ ferroelectric ceramics. Ceram. Int. **41**, 6055-6066 (2015).

[27] K. Ruan, A. Gao, W. Deng, X. Chen, D, Bao, Orientation dependent photoluminescent properties of chemical solution derived $Bi_{4-x}Eu_xTi_3O_{12}$ ferroelectric thin films. J. Appl. Phys. **104**, 036101 (2008).

[28] X. D. Li, Z. N. Chen, L. S. Sheng, Large enhancement of piezoelectric properties and resistivity in Cu/Ta co-doped $Bi_4Ti_3O_{12}$ high temperature piezoceramics. J. Am. Ceram. Soc. **102**, 7366-7375 (2019).

[29] S. K. Badge, A. V. Deshpande, Effect of vanadium doping on structural, dielectric and ferroelectric properties of bismuth titanate ($Bi_4Ti_3O_{12}$) ceramics. Ceram. Int. **45**, 15307-15313 (2019).

[30] X. Li, L. Zhu, P. Huang, Z. Chen, W. Bai, L. Li, F. Wen, P. Zhen, W. L. Wu, Y Zheng, Reduction of oxygen vacancy concentration and large enhancement of electrical performances in Cu/Sb co-doped $Bi_4Ti_3O_{12}$ high temperature piezoelectric ceramics. J. Appl.

Phys. **127**, 044102 (2020).

[31] Q. Zhou, B. J. Kennedy, C. Howard, Structural studies of the ferroelectric phase transition in $Bi_4Ti_3O_{12}$. Chem. Mater. **15**, 5025-5028 (2003).

[32] D. P. Song, J. Yang, J. X. Sun, L. Y. Chen, J. K. Lee, Controlling the crystallization of Nd-doped $Bi_4Ti_3O_{12}$ thin-films for lead-free energy storage capacitors. J. Appl. Phys. **127**, 224102 (2020).

[33] Y. Liu, L. Fan, W. Yi, C. Yan, J. Ma, Q. Ji, Q. Lin, Microstructure and ferroelectric properties of bi-excess $Bi_4Ti_3O_{12}$ thin films grown on Si and Pt/Ti/SiO_2/Si substrates. Ferroelectrics. **54**, 144-149 (2020).

[34] X. Du, W. Huang, S. K. Thatikonda, N. Qin, D. Bao, Improved ferroelectric and dielectric properties of Sm, La co-doped $Bi_4Ti_3O_{12}$ multifunctional thin films with orange-red emission. J. Mater. Sci.-Mater. El. **30**, 13158-13166 (2019).

[35] D, Coathup, Z. Li, X. Zhu, H. Yan, R. Zhang, H. Ye, Dielectric and ferroelectric properties of BTFCO thin films. J. Electroceram. **43**, 92-95 (2019).

[36] X. Hu, A. Garg, Z. H. Barber, Structural and electrical properties of samarium-substituted bismuth titanate ferroelectric thin films on Pt/TiOx/SiO_2/Si substrates. Thin. Solid. Films. **484**, 188-195 (2005).

[37] A. Xia, G. Tan, H. Ren, Effect of Fe substitution on microstructure and properties of bismuth titanate thin films. Ceram. Int. **42**, 1267-1271(2016).

[38] V. R. Prasad, M. Seshadri, S. Babu, Y. C. Ratnakaram, Concentration-dependent studies of Nd^{3+}-doped zinc phosphate glasses for NIR photoluminescence at 1.05 μm. Luminescence. **32**, 443-451 (2017).

[39] M. Balestrieri, S. Colis, M. Gallart, G. Schmerber, A. Dinia, Photoluminescence properties of rare earth (Nd, Yb, Sm, Pr)-doped CeO_2 pellets prepared by solid-state reaction. J. Mater. Chem. C. **3**, 7014-7021 (2015).

[40] I. M. Pinatti, T. M. Mazzo, R. F. Gonçalves, J. A. Varela, E. Longo, I. L. V. Rosa, $CaTiO_3$ and $Ca_{1-3x}Sm_xTiO_3$: photoluminescence and morphology as a result of hydrothermal microwave methodology. Ceram. Int. **42**, 1352-1360 (2016).

[41] S, Yang, J. Yao, Y. Quan, Monitoring the charge-transfer process in a Nd-doped semiconductor based on photoluminescence and SERS technology. Light.-Sci. Appl. **9**, 117 (2020).

[42] J. Y. Chen, C. H. Nie, Y. L. Bai, S. F. Zhao, The photovoltaic spectral response regulated by

band gap in Zr doped $Bi_4Ti_3O_{12}$ thin films. J. Mater. Sci.-Mater. El. **26**, 5917-5922 (2015).

[43] H. He, Z. He, Z. Jiang, J. Wang, T. Liu, N. Wang, A controllable photoresponse and photovoltaic performance in $Bi_4Ti_3O_{12}$ ferroelectric thin films. J. Alloy. Compd. **694**, 998-1003 (2017).

[44] L. Y. Chang, C. S. Tu, P. Y. Chen, Raman vibrations and photovoltaic conversion in rare earth doped $(Bi_{0.93}RE_{0.07})FeO_3$ (RE=Dy, Gd, Eu, Sm) ceramics. Ceram. Int. **42**, 834-842 (2016).

[45] S. Sharma, J. M. Siqueiros, O. R. Herrera, Structural, dielectric, ferroelectric and optical properties of Er doped $BiFeO_3$ nanoparticles. J. Alloy. Compd. **853**, 156979 (2021).

Figure Captions

Fig. 1 The preparation process of $Bi_{4-x}Nd_xTi_3O_{12}$ films.

Fig. 2 **a** The XRD patterns of $Bi_{4-x}Nd_xTi_3O_{12}$ films; **b** magnified diffraction peaks at about 30.0 °.

Fig. 3 The FESEM surface morphologies of $Bi_{4-x}Nd_xTi_3O_{12}$ films: **a** x=0; **b** x=0.25; **c** x=0.45; **d** x=0.65; **e** x=0.85.

Fig. 4 The FESEM cross-section morphologies of $Bi_{4-x}Nd_xTi_3O_{12}$ films: **a** x=0; **b** x=0.25; **c** x=0.45; **d** x=0.65; **e** x=0.85.

Fig. 5 The *P-E* hysteresis loops of $Bi_{4-x}Nd_xTi_3O_{12}$ films; inset: the values of *Pr* of $Bi_{4-x}Nd_xTi_3O_{12}$ films.

Fig. 6 The leakage current densities of $Bi_{4-x}Nd_xTi_3O_{12}$ films under different electric field; inset: the leakage current densities of $Bi_{4-x}Nd_xTi_3O_{12}$ films at 300 $KV\cdot cm^{-1}$.

Fig. 7 **a** Variation of dielectric constant with frequency for $Bi_{4-x}Nd_xTi_3O_{12}$ films ; **b** variation of dielectric loss with frequency for $Bi_{4-x}Nd_xTi_3O_{12}$ films.

Fig. 8 **a** The emission spectrum of $Bi_{4-x}Nd_xTi_3O_{12}$ films with different doped concentration of Nd^{3+}; **b** the excitation spectrum of $Bi_{4-x}Nd_xTi_3O_{12}$ films with different doped concentration of Nd^{3+}; **c** partial energy level diagram of Nd^{3+}.

Fig. 9 The diagrams of CIE chromaticity coordinate of $Bi_{4-x}Nd_xTi_3O_{12}$ films.

Fig. 10 **a** UV-Vis-NIR absorption spectra of $Bi_{4-x}Nd_xTi_3O_{12}$ films; **b** variation of $(\alpha hv)^{1/2}$ with hv.

Table Captions

Tab. 1 The ferroelectric parameters of $Bi_{4-x}Nd_xTi_3O_{12}$ films.

Tab. 2 The leakage current densities of $Bi_{4-x}Nd_xTi_3O_{12}$ films.

Tab. 3 *Eg* of $Bi_{4-x}Nd_xTi_3O_{12}$ films with different concentration of Nd^{3+}.

Figures

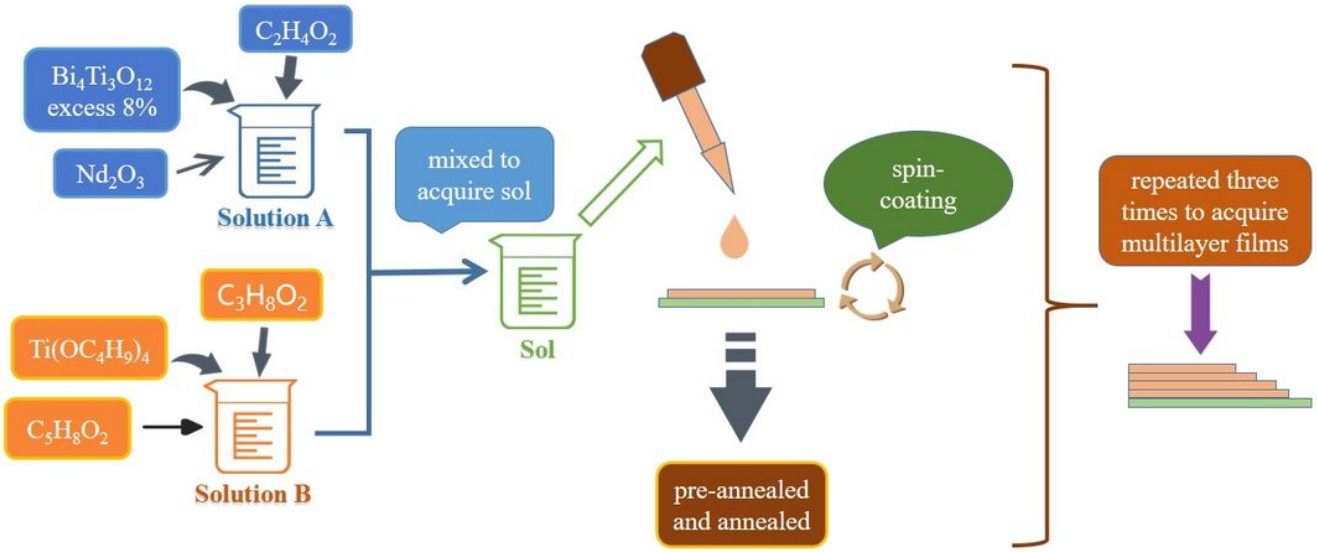

Figure 1

The preparation process of Bi4-xNdxTi3O12 films.

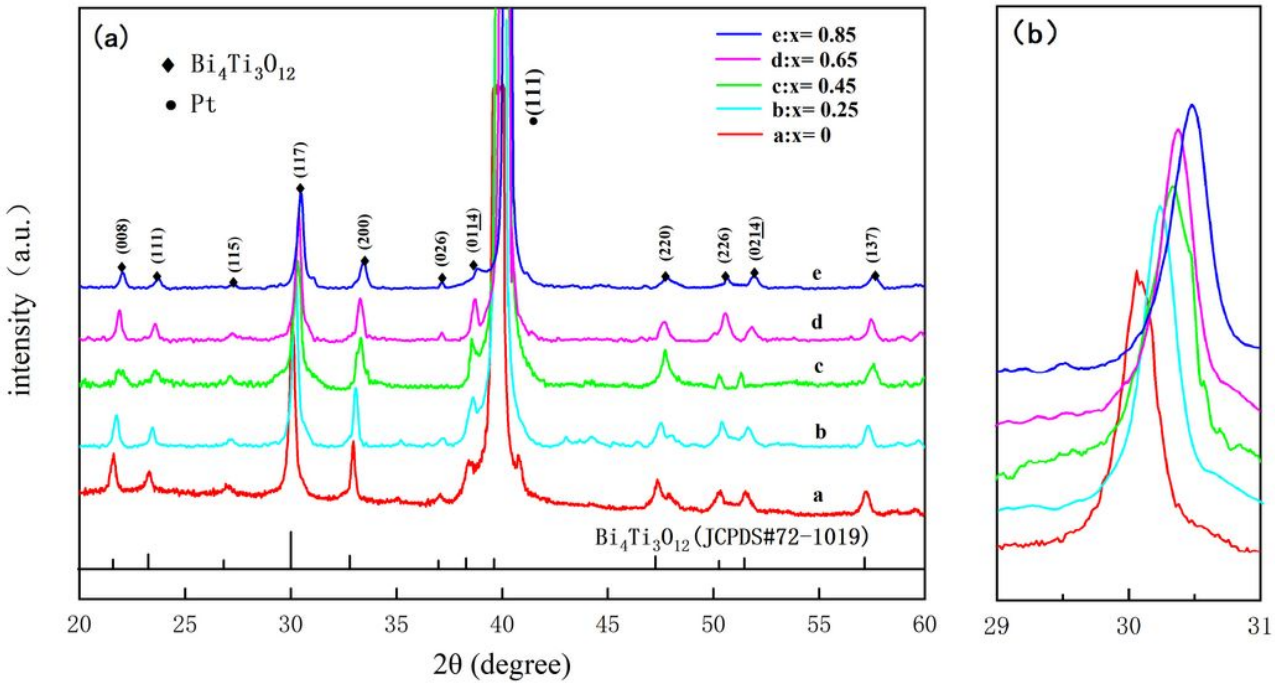

Figure 2

a The XRD patterns of Bi4-xNdxTi3O12 films; b magnified diffraction peaks at about 30.0 °.

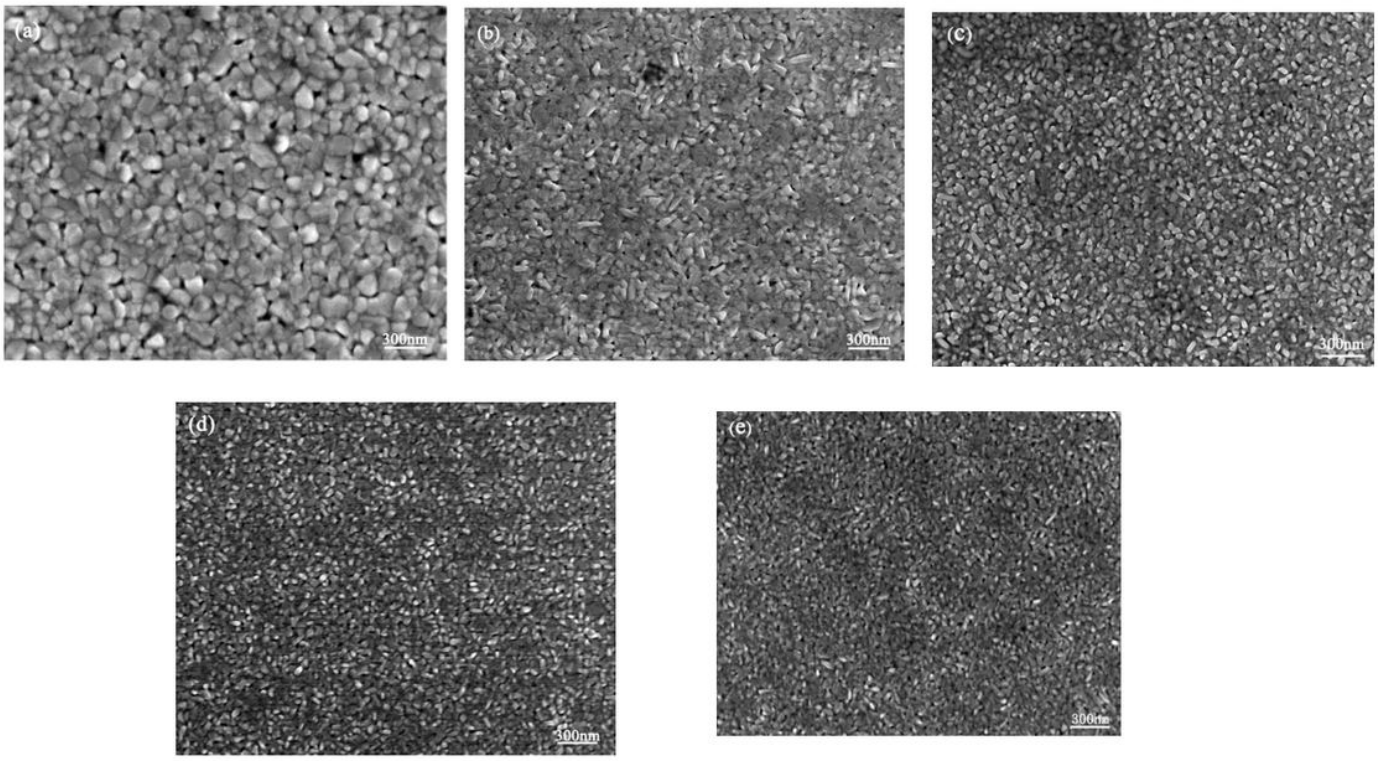

Figure 3

The FESEM surface morphologies of Bi4-xNdxTi3O12 films: a x=0; b x=0.25; c x=0.45; d x=0.65; e x=0.85.

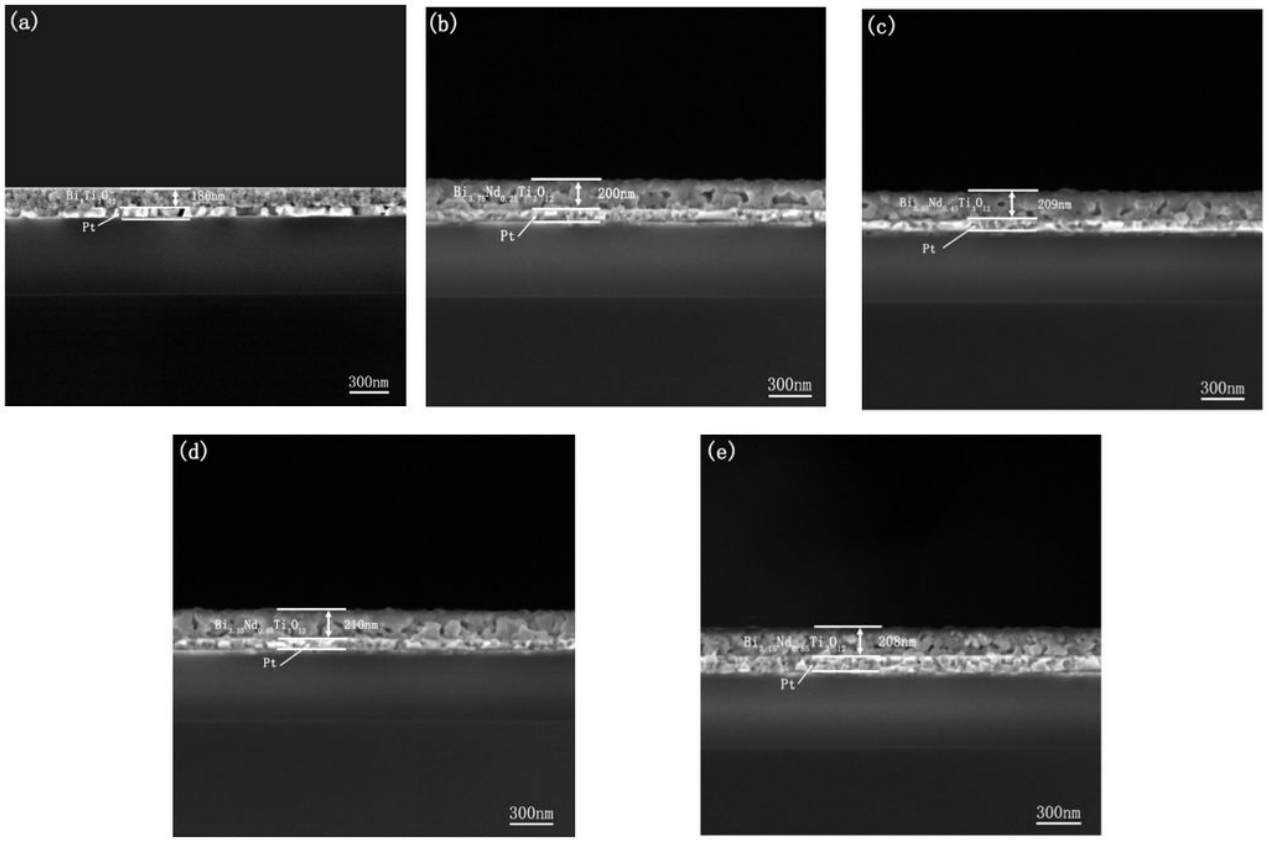

Figure 4

The FESEM cross-section morphologies of Bi4-xNdxTi3O12 films: a x=0; b x=0.25; c x=0.45; d x=0.65; e x=0.85.

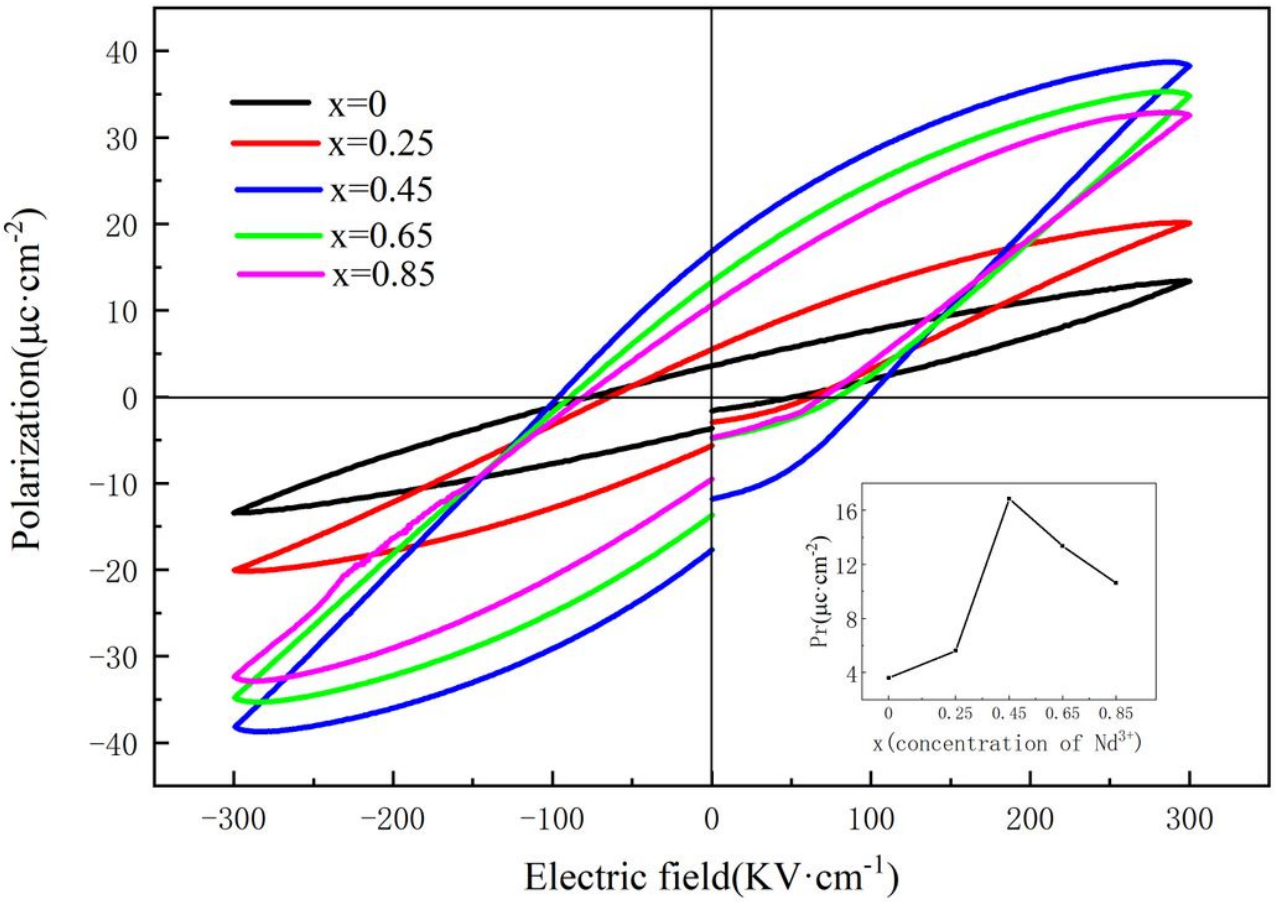

Figure 5

The P-E hysteresis loops of Bi4−xNdxTi3O12 films; inset: the values of Pr of Bi4−xNdxTi3O12 films.

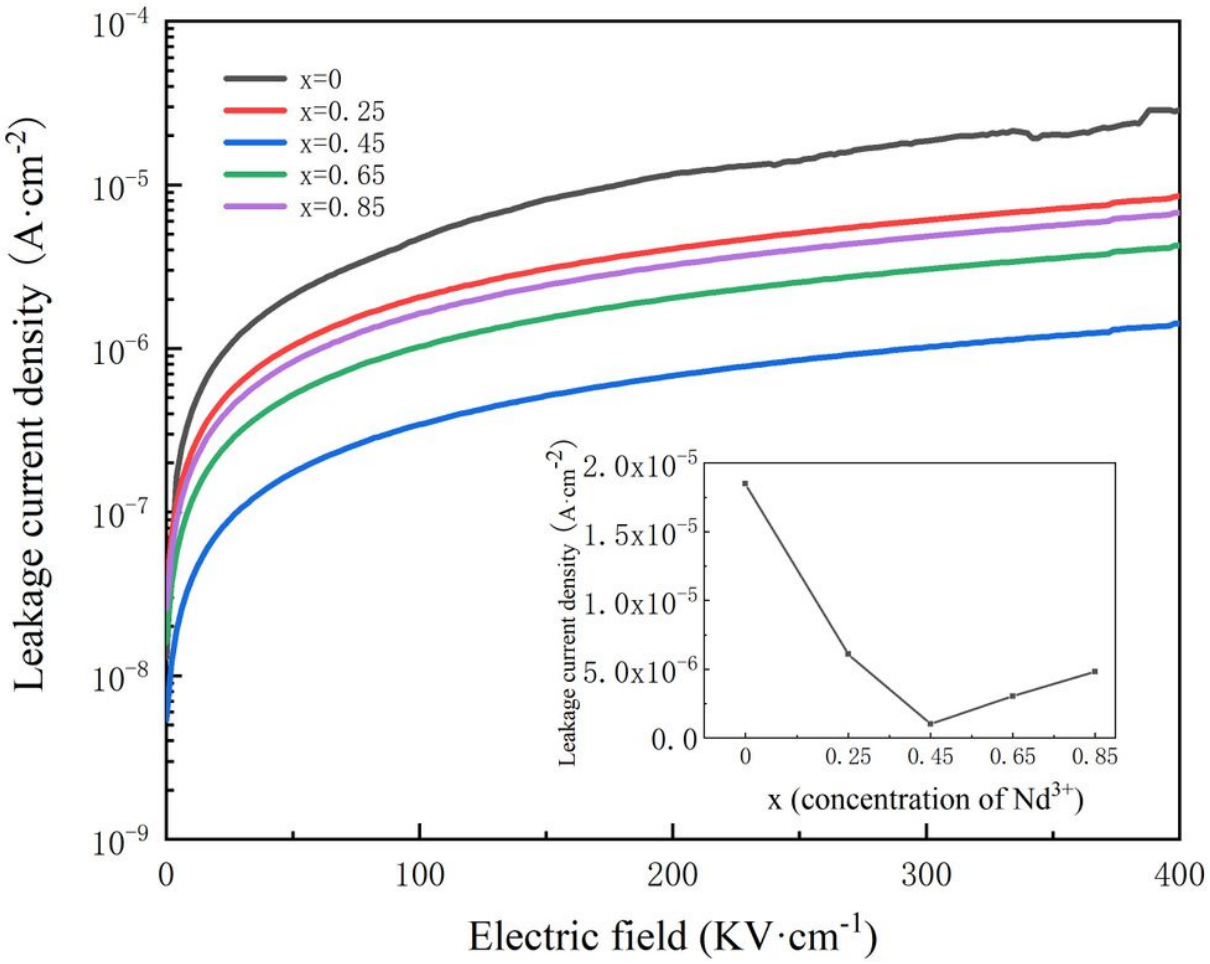

Figure 6

The leakage current densities of Bi4−xNdxTi3O12 films under different electric field; inset: the leakage current densities of Bi4−xNdxTi3O12 films at 300 KV·cm-1.

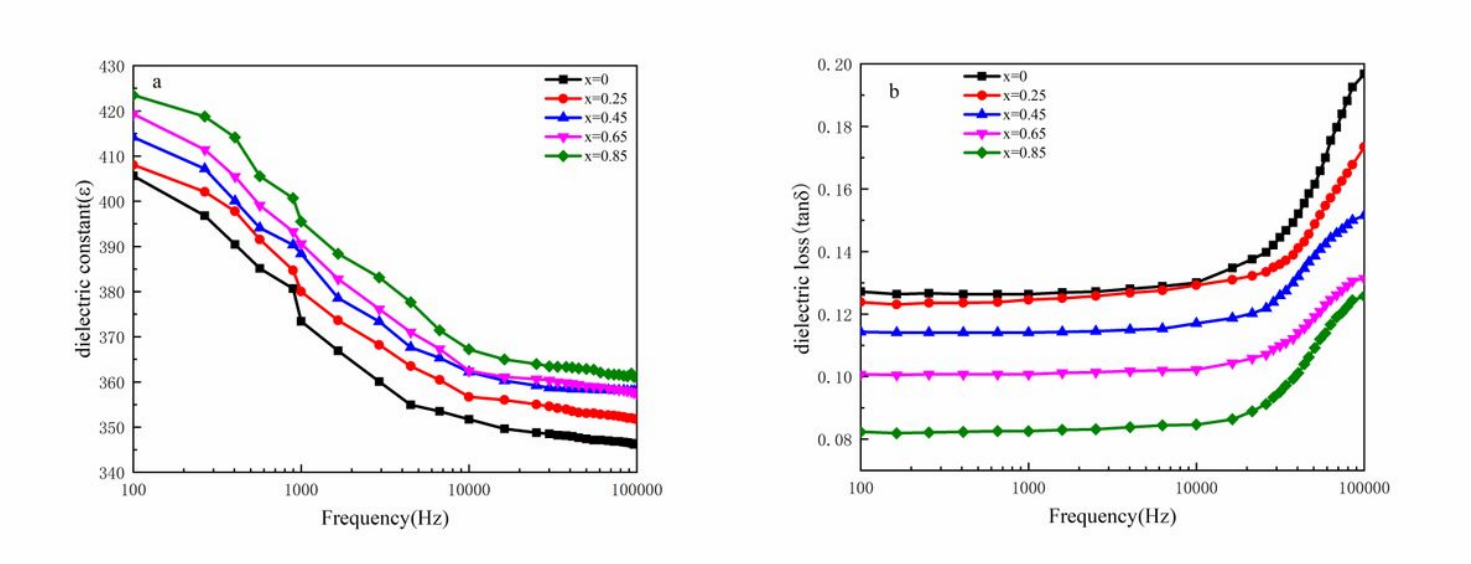

Figure 7

a Variation of dielectric constant with frequency for Bi4−xNdxTi3O12 films ; b variation of dielectric loss with frequency for Bi4−xNdxTi3O12 films.

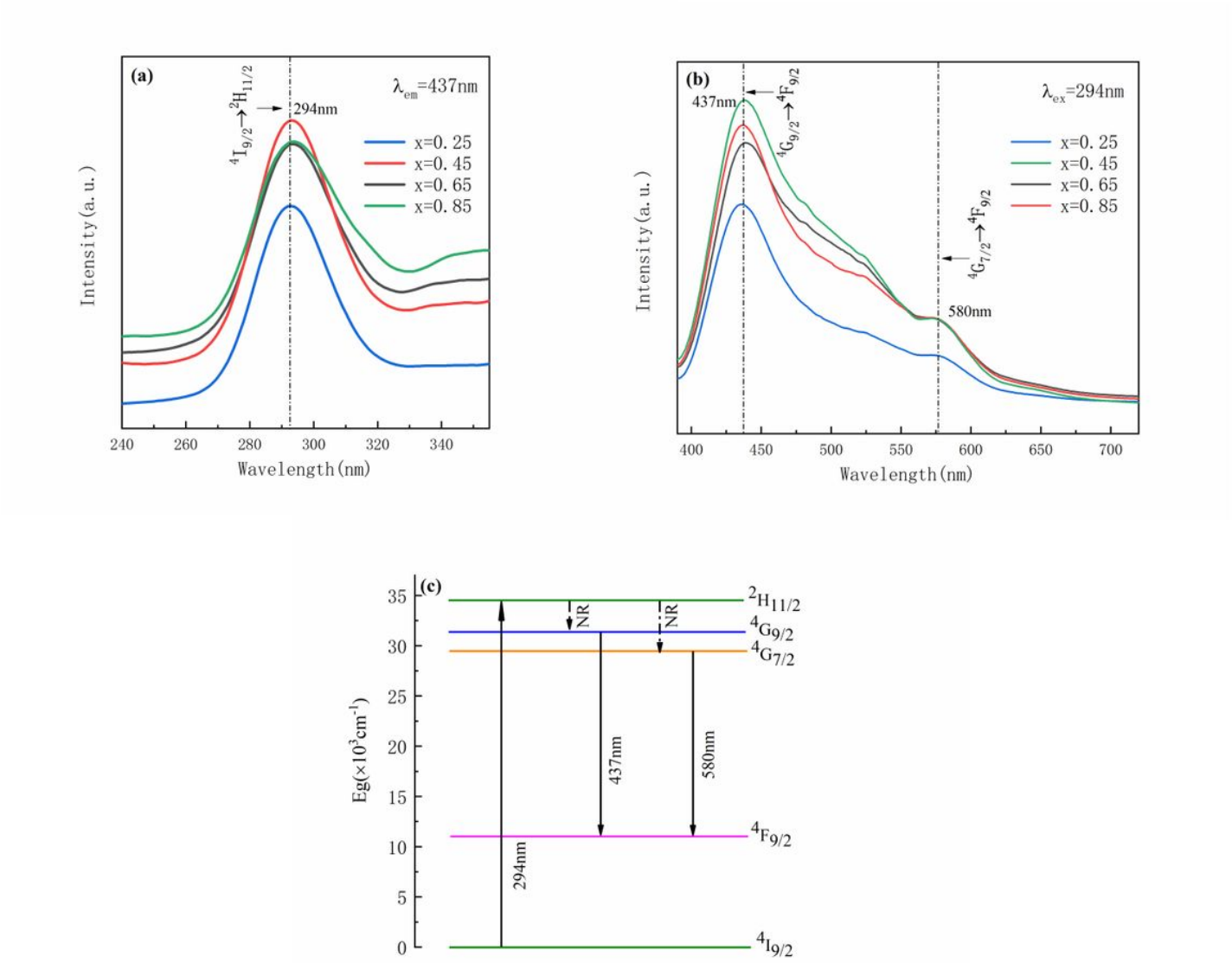

Figure 8

a The emission spectrum of Bi4−xNdxTi3O12 films with different doped concentration of Nd3+; b the excitation spectrum of Bi4−xNdxTi3O12 films with different doped concentration of Nd3+; c partial energy level diagram of Nd3+.

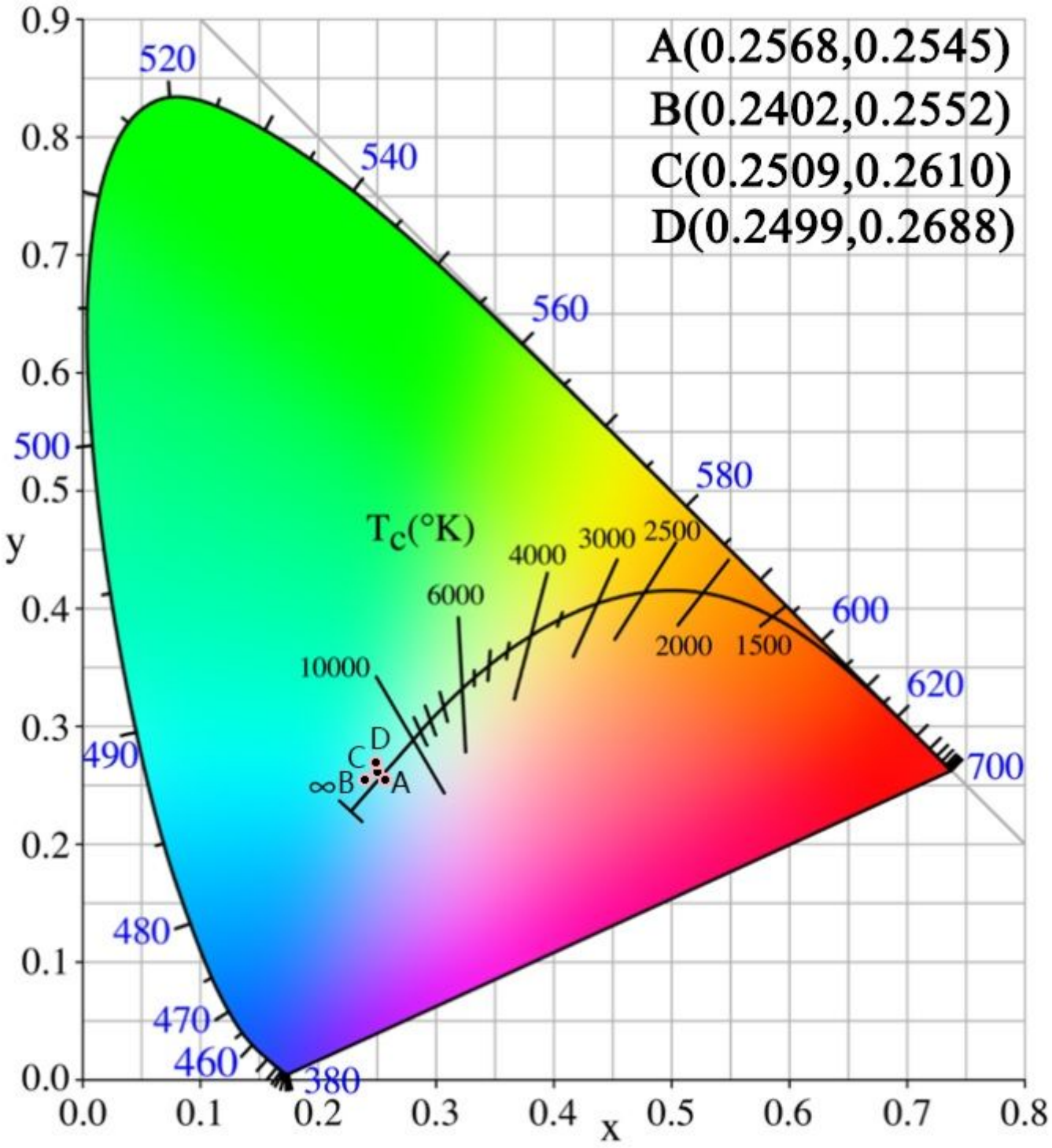

Figure 9

The diagrams of CIE chromaticity coordinate of Bi4-xNdxTi3O12 films.

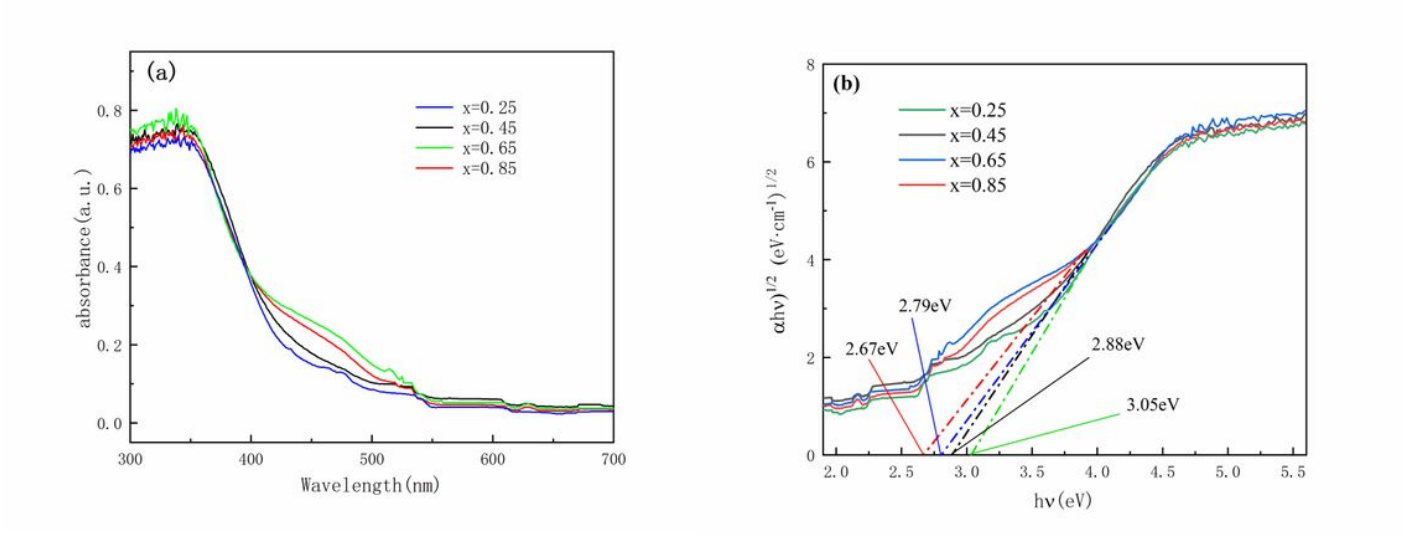

Figure 10

a UV-Vis-NIR absorption spectra of Bi4−xNdxTi3O12 films; b variation of (αhv)1/2 with hv.